A Combined Spectroelectrochemical and Computational Study of the Chemically Reversible 2-Electron Reduction of $[Ru_4(\mu\text{-}RC_2R)_2(CO)_{11}]$ Clusters

Olivia F. Koentjoro,[†] Paul J. Low,*[,†] Roger Rousseau,*[,‡] Carlo Nervi,[§] Dmitry S. Yufit,[†] Judith A. K. Howard,[†] and Konstantin A. Udachin[⊥]

Department of Chemistry, University of Durham, South Road, Durham, DH1 3LE, United Kingdom, International School for Advanced Studies, Via Beirut 4, 34014 Trieste, Italy, Dipartimento di Chimica IFM, Via P. Giuria, 10125 Torino, Italy, and Steacie Institute for Molecular Sciences, 100 Sussex Drive, Ottawa, Ontario, K1A 0R6, Canada

Received July 19, 2004

The 62-CVE clusters $Ru_4(\mu\text{-}RC_2R)_2(CO)_{11}$, which feature a dodecahedral cluster core, are readily reduced to a 64-CVE dianion in a process that is essentially chemically reversible. A combination of electrochemical, spectroelectrochemical, and computational analyses of the system indicates that the first formed dianion, which features a square planar arrangement of the metal centers with the alkyne ligands located on opposite faces of the M_4 square and oriented in a manner such that the C−C bonds are perpendicular to each other, undergoes a thermal rearrangement giving a product in which the alkyne vectors lie parallel to each other across the metal framework.

Introduction

Polyhedral metal clusters are interesting, and often robust, molecular species offering face, edge, and vertex sites for the attachment of ligands, and delocalized frontier orbitals derived from the bonding, nonbonding, and antibonding combinations of orbitals from the fragments that comprise the vertexes of the polyhedron. As a consequence of this structural and electronic versatility, the use of metal clusters as functional and structural units in the assembly of larger, more highly functionalized arrays is beginning to attract attention.[1]

In general terms, the introduction of additional electrons over and above the number required to populate the bonding and nonbonding molecular orbitals can lead to a general expansion of the cluster core or the elongation or cleavage of a specific M−M bond. In turn, this leads to a rich redox chemistry and the apt description of these materials as "electron sinks".[2] While there is considerable hope that cluster systems might prove feasible molecular components being developed as part of a molecular electronics kit,[3] in practice the electrochemical response of cluster systems is often complicated by chemical processes, such as loss of ligands such as CO from the cluster framework, which occur following the initial electrochemical event.

Here we describe the synthesis and structure and redox properties of the organometallic clusters $[Ru_4(\mu\text{-}RC_2R)_2(CO)_{11}]^{n-}$ ($n = 0, 2$) and show that the cluster core can be reversibly cycled between a 62-CVE (9 SEP) M_4C_4 dodecahedron and a 64-CVE M_4 square by electrochemical methods at moderate potentials with concomitant modifications to the electronic structure.

Results and Discussion

The thermal reactions of alkynes and polyynes with $Ru_3(CO)_{12}$ are sensitive to both the nature of the alkyne and the precise reaction conditions employed.[4] However, careful monitoring of reactions between $Ru_3(CO)_{12}$ and internal alkynes [PhC≡CPh (**1a**)] or 1,3,5-triynes [$Me_3Si(C{\equiv}C)_3SiMe_3$ (**1b**)] in refluxing hexane allows reasonable quantities of the clusters $Ru_4(\mu\text{-}RC_2R)(CO)_{12}$ [R = Ph (**2a**),[5] C≡CSiMe$_3$ (**2b**)[6]] to be obtained. These clusters, which are most likely formed by condensation of

* To whom correspondence should be addressed. Fax: +44 (0)191 384 4737. E-mail: p.j.low@durham.ac.uk.
[†] University of Durham.
[‡] International School for Advanced Studies.
[§] Dipartimento di Chimica IFM.
[⊥] Steacie Institute for Molecular Sciences.

(1) (a) Gorman, C. B.; Parkhurst, B. L.; Chen, K.-Y.; Su, W. Y. *J. Am. Chem. Soc.* **1997**, *119*, 1141. (b) Gorman, C. B.; Su, W. Y.; Jiang, H.; Watson, C. M.; Boyle, P. *Chem. Commun.* **1999**, 877. (c) Wang, R.; Zheng, Z. *J. Am. Chem. Soc.* **1999**, *121*, 3549. (d) Roland, B. K.; Carter, C.; Zheng, Z. *J. Am. Chem. Soc.* **2002**, *124*, 6234. (e) Feeder, N.; Geng, J.; Goh, P.; Johnson, B. F. G.; Martin, C. M.; Shepard, D. S.; W. Zhou, *Angew. Chem., Int. Ed.* **2000**, *39*, 1661. (f) Constable, E. C.; Eich, O.; Fenske, D.; Housecroft, C. E.; Johnston, L. A. *Chem. Eur. J.* **2000**, *6*, 4364. (g) Benito, M.; Rossell, O.; Seco, M.; Segalés, G. *Organometallics* **1999**, *18*, 5191. (h) Zheng, H.; Newkome, G. R.; Hill, C. L. *Angew. Chem., Int. Ed.* **2000**, *39*, 1772. (i) Lee, K.; Song, H.; Kim, B.; Park, J. T.; Park, S.; Choi, M.-G. *J. Am. Chem. Soc.* **2002**, *124*, 2872.

(2) Longoni, G.; Femoni, C.; Iapalucci, M. C.; Zanello, P. In *Metal Clusters in Chemistry*; Braunstein, P., Oro, L. A., Raithby, P. R., Eds.; Wiley-VCH: Weinheim, 1999; Vol 2, Chapter 3.9.

(3) See, for example: (a) Tour, J. M. *Acc. Chem. Res.* **2000**, *33*, 791. (b) Donhauser, Z. J.; Mantooth, B. A.; Kelly, K. F.; Bumm, L. A.; Monnell, J. D.; Stapleton, J. J.; Price, D. W., Jr; Rawlett, A. M.; Allara, D. L.; Tour, J. M.; Weiss, P. S. *Science* **2001**, *292*, 2303. (c) Dirk, S. M.; Price, D. W., Jr; Chanteau, S.; Kosynkin, D. V.; Tour, J. M. *Tetrahedron* **2001**, *57*, 5109. (d) Paul, F.; Lapinte, C. *Coord. Chem. Rev.* **1998**, *178−180*, 431. (e) Launay, J.-P.; Coudret, C. In *Electron Transfer in Chemistry*; Balzani, V., de Silva, A. P., Eds.; Wiley-VCH: New York, 2000; Vol. 5. (f) Ward, M. D. *J. Chem. Educ.* **2001**, *78*, 321.

(4) (a) Bruce M. I. In *Comprehensive Organometallic Chemistry*; G. Wilkinson, F. G. A. Stone, E. W. Abel, Eds.; Pergamon: Exeter, UK, 1982; Vol. 4, Chapters 32.5.2.9 and 32.6.1.2. (b) Low, P. J.; Bruce, M. I. *Adv. Organomet. Chem.* **2002**, *48*, 71.

10.1021/om049457y CCC: $30.25
Publication on Web 02/15/2005

Scheme 1

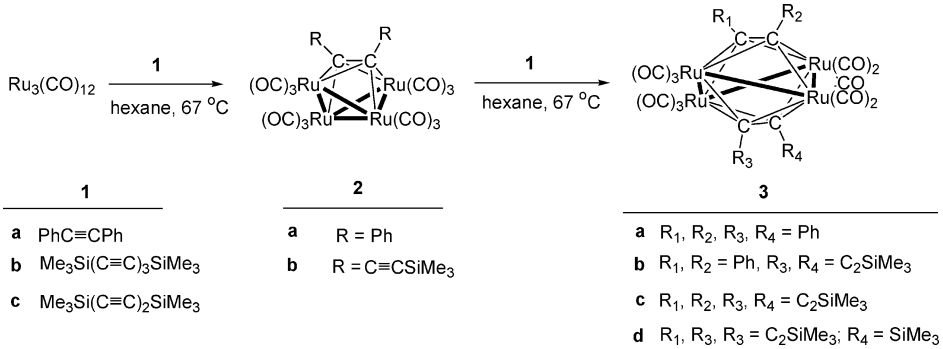

1

- **a** PhC≡CPh
- **b** $Me_3Si(C{\equiv}C)_3SiMe_3$
- **c** $Me_3Si(C{\equiv}C)_2SiMe_3$

2

- **a** R = Ph
- **b** R = C≡CSiMe₃

3

- **a** R_1, R_2, R_3, R_4 = Ph
- **b** R_1, R_2 = Ph, $R_3, R_4 = C_2SiMe_3$
- **c** $R_1, R_2, R_3, R_4 = C_2SiMe_3$
- **d** $R_1, R_3, R_3 = C_2SiMe_3$; R_4 = $SiMe_3$

$Ru_3(\mu_3\text{-}RC_2R')(CO)_{10}$ with an $Ru(CO)_n$ fragment generated in situ,[6,7] are easily separated from the other products by column chromatography or preparative TLC. Unreacted $Ru_3(CO)_{12}$ is readily recovered from the cooled reaction mixtures as a crystalline precipitate of high purity, which may be recycled in subsequent reactions.

Further reaction of **2a** with an equivalent of **1a** or **1b** in refluxing hexane gave $Ru_4(\mu_4\text{-}PhC_2Ph)_2(CO)_{11}$ (**3a**)[8] and $Ru_4(\mu_4\text{-}PhC_2Ph)(\mu_4\text{-}Me_3SiC{\equiv}CC_2C{\equiv}CSiMe_3)(CO)_{11}$ (**3b**), respectively, by insertion of the alkyne into the "hinge" of the Ru_4 butterfly-like fragment and loss of CO. Complex **3b** was also obtained from the reaction of **2b** with **1a**. Reaction of **2b** with **1b** or $Me_3Si(C{\equiv}C)_2SiMe_3$ (**1c**) gave $Ru_4(\mu_4\text{-}Me_3SiC{\equiv}CC_2C{\equiv}CSiMe_3)_2(CO)_{11}$ (**3c**) or $Ru_4(\mu_4\text{-}Me_3SiC{\equiv}CC_2C{\equiv}CSiMe_3)(\mu_4\text{-}Me_3SiC_2C{\equiv}CSiMe_3)(CO)_{11}$ (**3d**), respectively (Scheme 1). Cluster **3a** has also been obtained (18%) from the low-temperature trimethylamine-*N*-oxide (TMNO)-assisted reaction of $Ru_3(CO)_{12}$ and diphenyl acetylene.[8] Similar clusters, such as $Ru_4(\mu\text{-}MeC_2Ph)_2(CO)_{11}$ (**3e**)[9] and the parent cluster $Ru_4(\mu\text{-}HC_2H)_2(CO)_{11}$ (**3f**),[10] have been prepared on previous occasions by others.

The IR spectra of the clusters **3** were characterized by a series of terminal ν(CO) bands in the region 2000−1900 cm^{-1}, in addition to broad bands near 1850 cm^{-1} indicative of bridging carbonyl ligands. The free alkyne moieties in **3b**−**d** gave rise to $\nu(C{\equiv}C)$ bands between 2050 and 2100 cm^{-1}. The ^1H NMR contained the expected resonances from the protons of the C_6H_5 and $SiMe_3$ groups. The ^{13}C NMR spectra revealed a single broad peak near 200 ppm for the carbonyl ligands, which are rendered equivalent on the NMR time scale by rapid intramolecular exchange processes involving the migration of all the carbonyl groups around the tetraruthenium plane in a merry-go-round process,[9] as well as the usual resonances from the aromatic, acetylenic, and trimethylsilyl pendent groups as appropriate. The carbon nuclei of the Ru_4C_4 core were detected as sharp singlets between 110 and 150 ppm, depending upon substituent. Mass spectra (FAB ionization) contained the anticipated molecular ions, with fragment ions derived from the sequential loss of carbonyl ligands.

Molecular Structures. The molecular structures of **3b** (Figure 1) and **3d** (Figure 2) have been determined (Table 1) and may be compared with the structures of **3a**,[8] **3e**,[9] and the parent complex **3f** [10] (Table 2). The clusters **3** feature 9 skeletal electron pairs (SEP), or 62 cluster valence electrons (CVE), and therefore contain *closo*-dodecahedral Ru_4C_4 cluster cores. The gross structural features across the series are similar, and in all cases the metal centers sit ±0.31−0.34 Å from the mean least squares plane that passes through them. In the solid state, **3f** carries two μ-CO ligands located on adjacent Ru−Ru edges, while **3a** and **3e** each feature 10 terminal and one bridging carbonyl ligand. The Ru−Ru bond lengths in these previously characterized examples fall in the range 2.73−2.87 Å, with the shorter bonds being associated with the μ-CO ligands. The C−C bond lengths reflect the interactions with the metals and

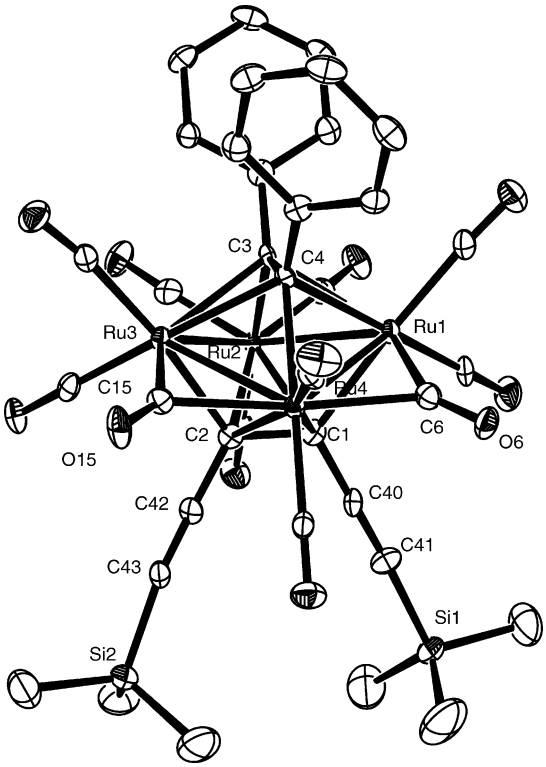

Figure 1. Plot of one molecule of **3b** showing the atom-labeling scheme. Hydrogen atoms have been omitted for clarity.

(5) (a) Johnson, B. F. G.; Lewis, J.; Schorpp, K. T. *J. Organomet. Chem.* **1975**, *91*, C13. (b) Johnson, B. F. G.; Lewis, J.; Reichert, B. E.; Schorpp, K. T.; Sheldrick, G. M. *J. Chem. Soc., Dalton Trans.* **1977**, 1417.

(6) Low, P. J.; Udachin, K. A.; Enright, G. D.; Carty, A. J. *J. Organomet. Chem.* **1999**, *578*, 103.

(7) Adams, R. D.; Bunz, U. H. F.; Fu, W.; Roidl, G. *J. Organomet. Chem.* **1999**, *578*, 55.

(8) Davies, J. E.; Johnson, B. F. G.; Martin, C. M.; Pearson, R. H. H.; Dyson, P. J. *J. Organomet. Chem.*, **1998**, *550*, 431.

(9) Aime, S.; Nicola, G.; Osella, D.; Lanfredi, A. M. M.; Tiripicchio, A. *Inorg. Chim. Acta* **1984**, *85*, 161.

(10) Bruce, M. I.; Zaitseva, N. N.; Skelton, B. W.; White, A. H. *J. Chem. Soc., Dalton Trans.* **2002**, 3879.

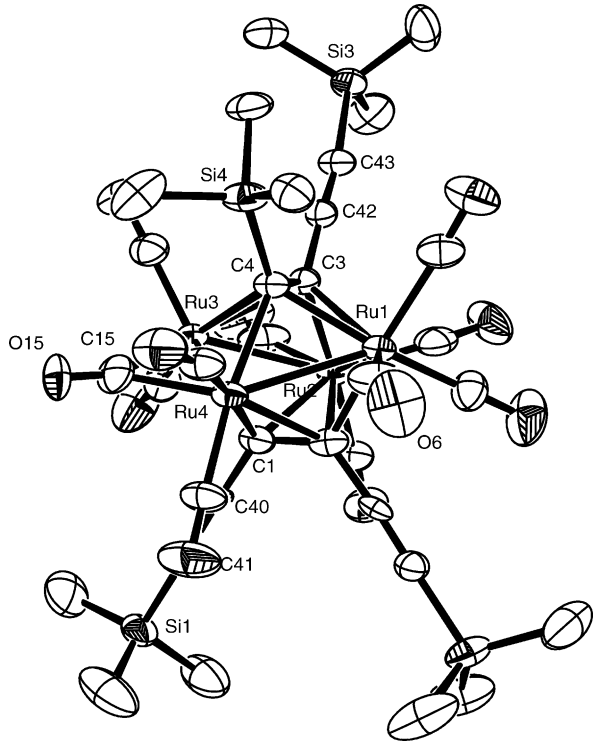

Figure 2. Plot of **3d** showing the atom-labeling scheme. Hydrogen atoms have been omitted for clarity.

are considerably longer than the C≡C bonds in free alkynes, while for the most part the Ru−C bond lengths fall into two distinct ranges, lying between 2.12 and 2.19 Å and from 2.30 to 2.50 Å.

The solid state structure of **3b** contains two independent molecules which differ in the arrangement of the carbonyl ligands around the Ru_4C_4 core and the pattern of metal−metal bond lengths. Molecule 1 contains two semibridging carbonyl groups [Ru(3)−C(15) 2.010(5); Ru(4)−C(15) 2.218(5) Å; Ru(3)−C(15)−Ru(4) 80.8(2)°; Ru(4)−C(6) 2.184(5); Ru(1)−C(6) 2.024(5) Å; Ru(4)−C(6)−Ru(1) 81.8(2)°] spanning the adjacent edges Ru(3)−Ru(4) [2.7448(5) Å] and Ru(4)−Ru(1) [2.7567(6) Å]. The other Ru−Ru bond lengths are considerably longer [Ru(3)−Ru(2) 2.8462(6), Ru(2)−Ru(1) 2.8815(6) Å]. The Ru−C(cluster) bond lengths fall within the range 2.147(5)−2.221(5) Å and 2.273(5)−2.418(5) Å. Molecule 2 contains a single bridging carbonyl ligand [Ru(3)−C(15) 2.053(6); Ru(4)−C(15) 2.090(6) Å; Ru(3)−C(15)−Ru(4) 83.0(2)°] spanning the shortest Ru−Ru bond [Ru(3)−Ru(4) 2.7453(6) Å cf. Ru(4)−Ru(1) 2.8124(7), Ru(2)−Ru(1) 2.8339(6), Ru(2)−Ru(3) 2.8530 Å]. The Ru−C(cluster) bond lengths cover a slightly greater range than displayed in the previous examples, with Ru−C bonds in the ranges 2.122(6)−2.208(6) Å and 2.267(5)−2.430(6)Å.

The molecular parameters associated with the Ru_4C_4 cluster core of **3d** are similar to those of the other examples in the series, with Ru−Ru bond lengths spanning the range 2.7583(2)−2.8521(3) Å and Ru−$C_{cluster}$ bond lengths between 2.216(1) and 2.296(1) Å. Of the 11 carbonyl ligands, two adopt μ_2-bridging modes.

Electrochemistry and IR Spectroelectrochemistry. The cyclic voltammetric (CV) response of dichloromethane solutions of **3a** and **3c** (Figure 3) were characterized by a single, two-electron, chemically irreversible reduction process (A) in each case [E_p(A): **3a** −1.528 V; **3c** −1.580 V vs Fc/Fc^+] with the reoxidation peak B [E_p(B): **3a** −0.650 V; **3c** −0.465 V vs Fc/Fc^+] appearing only as a consequence of the reduction A. Polarography of the same solutions showed only one reduction wave [$E_{1/2}$: **3a** −1.418 V; **3c** −1.387 V], and in each case logarithmic analysis gave a linear plot with a slope of 47 mV. This value is between that expected for a $1e^-$ (59 mV) and $2e^-$ reduction processes (29.5 mV). However, bulk electrolysis performed at a mercury-pool electrode at −1.60 V consumed exactly 2 F/mol, during which the initial red-orange solution turned yellow. Bulk reoxidation at +0.30 V also consumed 2 F/mol and restored the initial red-orange color to the solution.

Curiously, the cyclic voltammogram of the yellow electrolysis solution was characterized by two one-electron oxidation waves [$E_{1/2}$(C) **3a** −0.605 V, **3c** −0.419 V; and $\mathbf{E}_{1/2}$(D) **3a** −0.100 V, **3c** +0.095 V), which were not electrochemically reversible on the time scale of the CV experiment. Therefore, the clusters **3** are reduced in a single two-electron event to give a dianion, $\mathbf{3}^{2-}$, which can be reoxidized in a single two-electron process on the CV time scale. On longer time scales, $\mathbf{3}^{2-}$ converts to a second species, $\mathbf{4}^{2-}$, via a non-electrochemical process. Compound $\mathbf{4}^{2-}$ is reoxidized in two sequential one-electron steps and ultimately reverts to **3** (Scheme 2). The overall mechanism (EECEEC) is sketched in Scheme 2, where the second reduction of **3** is more thermodynamically favorable than the first, $E°_3(-1/-2) > E°_3(0/-1)$ (total of 2e reduction), and the kinetics of the heterogeneous electron transfers are generally slow (quasi-reversible electrochemical electron transfer). In keeping with this suggestion, we note if

Table 1. Crystal Data for Compounds 3b and 3d

	3b	**3d**
empirical formula	$C_{37}H_{28}O_{11}Ru_4Si_2$	$C_{33}H_{36}O_{11}Ru_4Si_4$
fw (g/mol)	1109.05	1125.26
temperature (K)	120(2)	173(2)
cryst syst	monoclinic	monoclinic
space group	$P2_1/c$	Cm
a (Å)	27.2520(9)	13.5503(8)
b (Å)	9.5309(3)	13.7423(9)
c (Å)	33.374(1)	12.3319(7)
β (deg)	108.51(1)	101.09(1)
V (Å^3)	8219.9(4)	2253.3(2)
Z	8	2
ρ (mg/m^3)	1.792	1.658
μ (mm^{-1})	1.555	1.470
no. of reflns collected (indep)	65 769 (18 870)	13 383 (6019)
R indices (all data)	R_1 0.0786, wR_2 0.1029	R_1 0.0487, wR_2 0.0645
largest diff peak and hole (e Å^{-3})	2.149, −0.916	0.673, −0.460

Table 2. Selected Bond Lengths for Experimental Compounds 3a, 3b, 3d, and 3f and Computational Models 3f, $3f^{2-}$, and $4f^{2-}$

	3a[8a]		**3b**						
	mol 1	mol 2	mol 1	mol 2	**3d**	**3f**[10a]	**3f**[b]	$3f^{2-b}$	$4f^{2-b}$
Ru(1)−Ru(4)	2.8716(7)	2.8658(7)	2.7567(6)	2.8339(6)	2.8521(3)	2.7732(14)	2.824	2.858	2.752
Ru(1)−Ru(2)	2.7618 (7)	2.7628(7)	2.8815(6)	2.8530(7)	2.7948(2)	2.8338(14)	2.865	2.866	3.144
Ru(2)−Ru(3)	2.8649 (7)	2.8692(7)	2.8462(6)	2.7452(6)	2.8386(2)	2.8338(14)	2.871	3.001	2.736
Ru(3)−Ru(4)	2.7656(7)	2.7668(7)	2.7448(5)	2.8123(7)	2.7583(2)	2.7732(14)	2.829	2.866	3.014
Ru(1)−C(1)	2.221(6)	2.198(6)	2.161(5)	2.122(6)	2.0432(10)	2.143(12)	2.159	2.209	2.187
Ru(1)−C(4)	2.339(6)	2.278(6)	2.303(5)	2.353(5)	2.2205(11)	2.72(10)	2.333	2.177	3.093
Ru(1)−C(3)	2.273(6)	2.365(6)	2.419(5)	2.350(6)	2.2626(11)	2.312(12)	2.402	2.995	2.215
Ru(2)−C(3)	2.210(6)	2.207(6)	2.147(5)	2.208(6)	2.1878(18)	2.11(2)	2.121	2.183	3.010
Ru(2)−C(1)	2.365(5)	2.329(6)	2.273(5)	2.318(6)	2.2961(10)	2.310(15)	2.360	2.184	2.956
Ru(2)−C(2)	2.275(6)	2.288(6)	2.290(5)	2.267(5)	2.2961(10)	2.310(15)	2.351	2.995	3.308
Ru(3)−C(2)	2.192(6)	2.189(6)	2.150(5)	2.170(6)	2.2783(10)	2.143(12)	2.163	2.184	2.237
Ru(3)−C(4)	2.498(6)	2.484(6)	2.351(5)	2.430(6)	2.4177(11)	2.272(10)	2.340	2.952	2.175
Ru(3)−C(3)	2.311(5)	2.320(6)	2.397(5)	2.344(6)	2.3294(9)	2.312(12)	2.394	2.185	3.022
Ru(4)−C(4)	2.180(6)	2.195(6)	2.220(5)	2.171(5)	2.2229(17)	2.138(16)	2.163	2.177	2.988
Ru(4)−C(2)	2.514(6)	2.478(6)	2.310(5)	2.273(6)	2.2161(10)	2.283(12)	2.365	2.209	2.942
Ru(4)−C(1)	2.306(6)	2.334(5)	2.328(5)	2.358(6)	2.4123(11)	2.283(12)	2.369	2.981	2.229
C(1)−C(2)	1.406(8)	1.420(8)	1.428(7)	1.428(8)	1.426(2)	1.366(17)	1.389	1.401	1.397
C(3)−C(4)	1.407(8)	1.425(8)	1.422(7)	1.509(8)	1.416(2)	1.39(3)	1.395	1.428	1.403
diff from mean plane									
Ru(1)	+0.3350	−0.3293	+0.3409	−0.3312	+0.3727		+0.3124	0	+0.033
Ru(2)	−0.3345	+0.3287	−0.3280	+0.3433	−0.3799		−0.3066	0	−0.033
Ru(3)	+0.3340	−0.3296	+0.3473	−0.3486	+0.3799		+0.3112	0	+0.033
Ru(4)	0.3345	+0.3301	−0.3602	+0.3364	−0.3781		−0.3170	0	−0.033

[a] Experimental data, reported using atom labeling as depicted in Figures 1 and 2. [b] Calculated values.

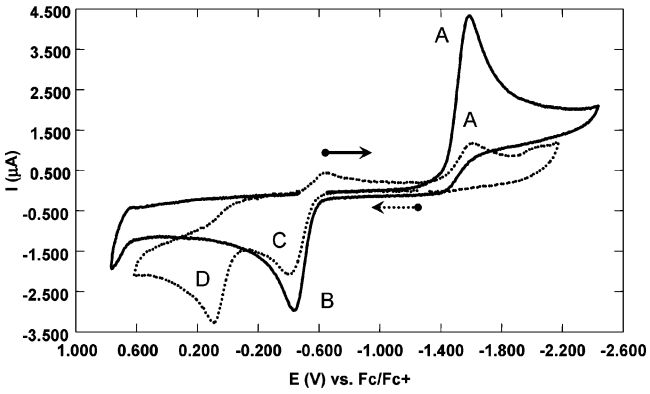

Figure 3. CV response of **3c** (dark trace) and after bulk electrolytic reduction (light trace).

Scheme 2. E/C Cycle Associated with the Electrochemical Response of Clusters 3

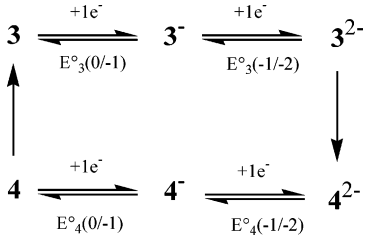

the electrolysis is carried out at low temperatures, the conversion of 3^{2-} to 4^{2-} is significantly retarded, and the electrochemical response of solutions following electrolysis at low temperature are similar to those of the initial solution. For instance, in the case of compound **3a**, while at room temperature the peak-to-peak separation of the electrochemically quasi-reversible reduction process is about 0.88 V. This separation become much wider at −80 °C (1.31 V). This is consistent with the proposed heterogeneous electrochemical sluggishness induced by geometrical rearrangement, since its kinetics should undergo a substantial decrease due to the lowering of the temperature. Simulations (ESP) of the EECEEC mechanism are in agreement with the experimental data (see Supporting Information).

Infrared spectroelectrochemical studies were carried out to gain some insight into the chemical processes occurring during the electrochemical cycle. The ν(CO) patterns of **3a** and **3c** in 1,2-dichloroethane containing 0.1 M NBu_4PF_6 supporting electrolyte were similar to the spectra in cyclohexane. In situ reduction caused the ν(CO) and ν(C≡C) absorption bands characteristic of **3a**/**3c** to collapse, giving way to a new set of bands associated with the most thermodynamically stable form of the electrochemically generated dianion [$\mathbf{4a}^{2-}$ ν(CO) 1953 vs, 1897 m, 1749 w cm^{-1}; $\mathbf{4c}^{2-}$ ν(C≡C) 2107 w, ν(CO) 1962 vs, 1903 m, 1751 w cm^{-1}] (Figure 4). The decrease in the stretching frequencies of the predominant carbonyl bands following reduction is consistent with the greater electron density associated with the dianions. The original spectrum was almost entirely recovered upon reoxidation. The spectroelectrochemical behavior was identical under atmospheres of N_2 or CO, and given the regeneration of the starting complexes after the reduction/reoxidation cycle carbonyl dissociation or cluster fragmentation processes are not likely to be associated with the electrochemical reduction.

Computational Analysis. A computational study of the redox cycle observed for **3a** and **3c** using $Ru_4(CO)_{11}(\mu_4\text{-}HC_2H)_2$ (**3f**) as a model was undertaken. Geometry optimization was performed as described in the Experimental Section, and selected bond lengths and angles are summarized in Table 2, along with the data relating to the crystallographically determined structures. While quantitative agreement between the observed and calculated data is not expected due the nature of the calculations and structural approximations involved, the optimized geometry of **3f** is in good general agreement with the experimentally observed structural trends, which allows for a high degree of confidence in the

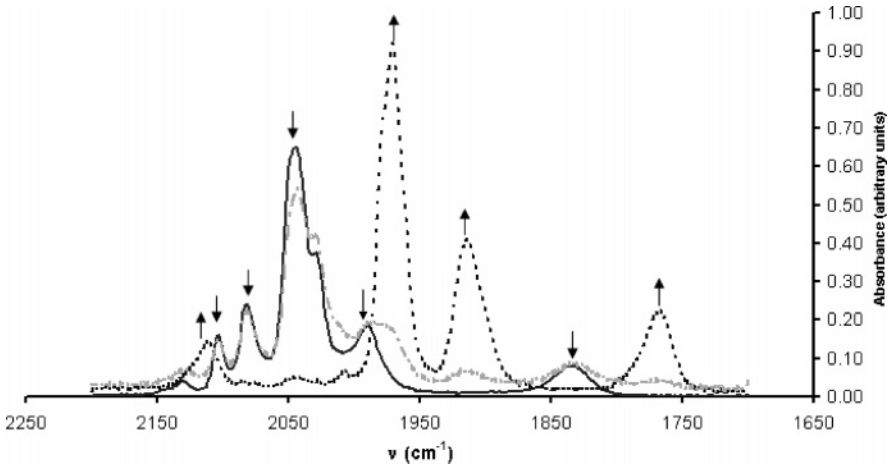

Figure 4. IR spectroelectrochemically response of **3c** Solid line: infrared spectrum of the starting solution of **3c**. Dashed line: after full reduction at −1.80 V. Dotted line: after reoxidation at +0.30 V.

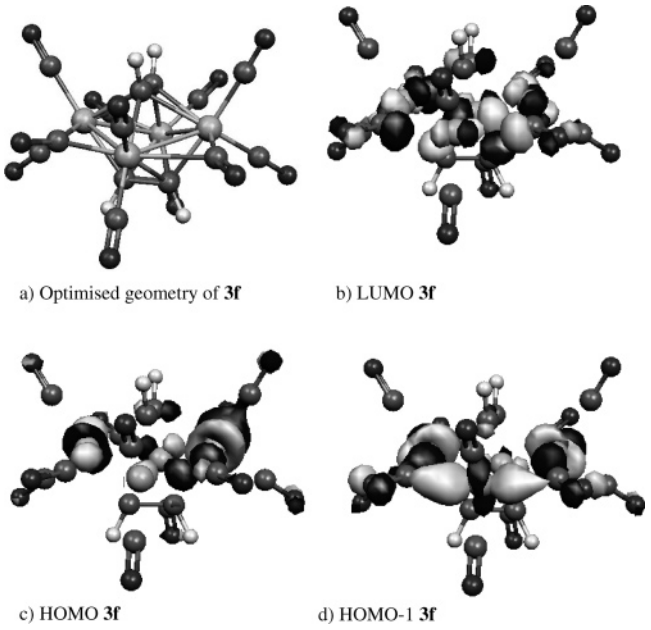

Figure 5. (a) Optimized geometry of **3f** along with associated (b) LUMO, (c) HOMO, and (d) HOMO−1.

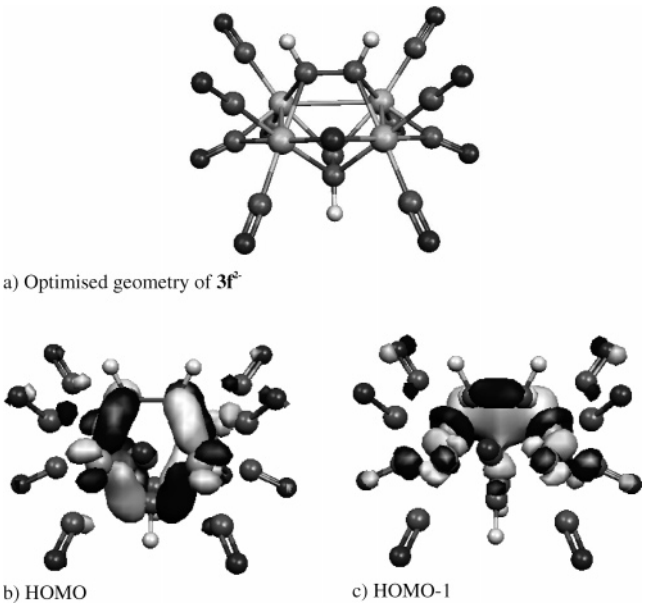

Figure 6. (a) Optimized geometry of $\mathbf{3f}^{2-}$ along with associated (b) HOMO and (c) HOMO−1.

accuracy of the computations and the conclusions drawn from them.

The geometry optimized model structure of **3f** presented the same gross structure as the experimentally determined structures, with the four metal centers forming a puckered square arrangement and the alkyne moieties oriented diagonally across opposite corners, giving the anticipated dodecahedral Ru_4C_4 core (Figure 5). Two of the carbonyl ligands are found bridging adjacent Ru−Ru bonds. The Ru−Ru bond lengths fall in the range 2.824−2.871 Å. The metal centers of the Ru_4 core are approximately ±0.31 Å from the mean least squares plane defined by them.

An analysis of the orbital structure of the cluster reveals the expected nest of low lying occupied orbitals derived from various combinations of the metal, carbonyl, and alkyne fragments. The HOMO and HOMO−1 are somewhat removed from the remainder of the occupied orbitals and of similar composition, consisting mainly of antibonding combinations of the d_{z^2} orbitals that make up the M−M σ-framework (Figure 5). The LUMO consists largely of Ru−Ru and Ru−C(alkyne) antibonding interactions.

To simulate the events occurring following reduction, the number of electrons in the structurally optimized model **3f** was increased by two to give the 10-SEP/64-CVE dianion $\mathbf{3f}^{2-}$, and the structure reoptimized (Figure 6). The four ruthenium centers in $\mathbf{3f}^{2-}$ define a planar rectangular structure, with the alkyne C−C vectors, which are mutually orthogonal, located above and below this plane and, in contrast to **3f**, parallel to two of the metal edges. The Ru_4C_4 core can therefore be described as two trigonal prisms fused orthogonally through the M_4 face. On the basis of electron-counting rules, and assuming each alkyne ligand donates four electrons, the 64-CVE dianion is described as a Ru_4 square cluster, which is entirely in agreement with the optimized geometry.

The core of the dianion $\mathbf{3f}^{2-}$ has three "normal" Ru−Ru bonds (2.858, 2.866, 2.866 Å) and one long one (3.001 Å), with the three bridging carbonyls spanning the shorter Ru−Ru bonds (Figure 6, Table 2). Each metal center also carries two terminal carbonyl ligands. The

Scheme 3

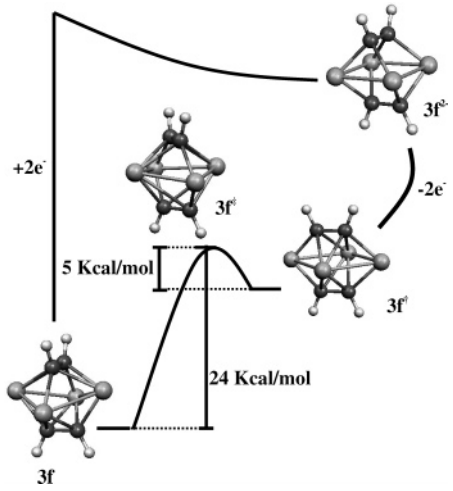

bridging form of the carbonyl ligand is more basic at the oxygen and more electron withdrawing with respect to the cluster than the terminal form.[11] The increased number of bridging carbonyls is therefore not surprising, as this provides an avenue to delocalize the excess charge in the dianion. On the basis of Mulliken population analysis of **3f** and **3f²⁻**, the additional electron density in **3f²⁻** is distributed over the Ru_4 centers ($0.4e^-$), the alkyne carbons ($0.1e^-$), and the carbonyl ligands ($1.5e^-$). The average metal−metal bond length in the dianion **3f²⁻** (2.89_8 Å) is only slightly longer than the average in the calculated structure of the neutral species (2.84_7 Å), while the Ru−C(alkyne) bond lengths fall in the range 2.177−2.209 Å (av 2.18_9 Å), consistent with the description of each in terms of a Ru−C σ-bond. The C−C bond lengths increase following reduction of the cluster from 1.389/1.395 Å in the optimized structure **3f** to 1.401/1.428 Å in the dianion **3f²⁻**. The HOMO and HOMO−1 of this species are essentially isoenergetic and somewhat removed from the remaining occupied orbitals. The HOMO of **3f²⁻** is essentially formed by mixing of a set of metal d-orbitals with the alkyne π^*-orbitals, giving an MO which is strongly Ru−C bonding and C−C antibonding, which accounts for the observed structural trends (Figure 6b). The HOMO−1 is essentially Ru−Ru bonding in character and localized on the non-carbonyl bridged bond, with a small, but significant, bonding interaction with the carbon orbitals of one of the alkyne ligands (Figure 6c).

To mimic the reoxidation event observed in the initial CV sweep, two electrons were removed from **3f²⁻** and the geometry reoptimized, affording a new structure, $Ru_4(CO)_{11}(\mu_4\text{-}HC_2H)_2$ (**3f†**), which resides in a local minimum on the potential energy surface associated with the neutral species (Scheme 3). In this intermediate structure, the alkyne vectors are parallel to each other and lie diagonally across the Ru_4 plane. The reaction pathway between **3f†** and **3f** was examined in some detail to clarify the relationship between these species. A transition state structure calculation was carried out, during which the transient species **3f‡** was identified. The core geometry in **3f‡** features an approximately square arrangement of the four metal atoms, which lie some ±0.12−0.13 Å from the mean

(11) Crabtree, R. H.; Lavin, M. *Inorg. Chem.* **1986**, *25*, 805.

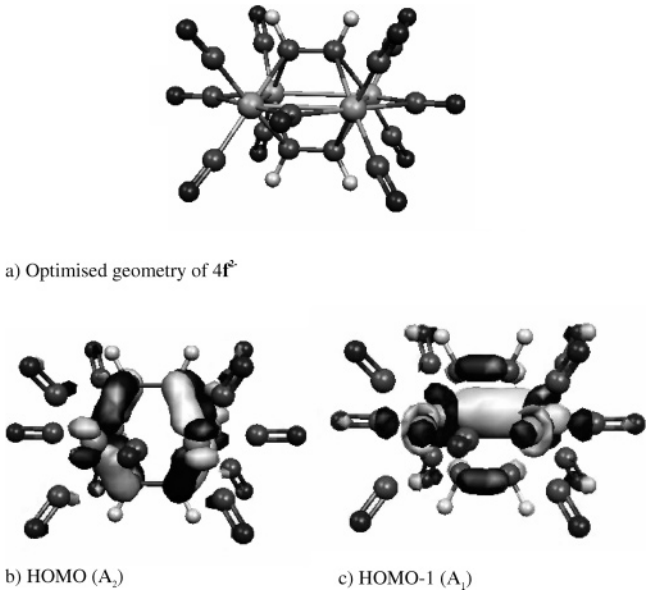

Figure 7. (a) Optimized geometry of **4f²⁻** with associated (b) HOMO and (c) HOMO−1.

least squares plane that passes through them. The alkyne vectors are twisted from the parallel arrangement in **3f†** but not yet at positions required by **3f**. An energy barrier of 5 kcal/mol was calculated for the forward reaction **3f†** → **3f**, while the barrier to the back reaction was calculated to be 24 kcal/mol. The changes in the metal atom framework that accompany the overall transformation **3f** → **3f²⁻** → **3f†** → **3f‡** → **3f** are shown schematically in Scheme 3.

Thus, initial reduction of the clusters **3** results in the consumption of two electrons per molecule (cf **3c**, Figure 3, wave A) and the formation of the square clusters **3²⁻**. This dianion is itself redox active, being reoxidized (Figure 3, waves B) to give an intermediate, **3†**, which is thermodynamically unstable with respect to **3**. Therefore, while the electrochemical events are chemically reversible, the geometrical changes that accompany the electrochemical processes suggest that the rate of electron transfer would not likely be diffusion controlled, and the cycle should be expected to be electrochemically irreversible, as observed.

The experimental electrochemistry shows the monoanion **3f⁻** to be unstable with respect to disproportiontion to **3f** and **3f²⁻**. It is rather difficult to address this point satisfactorily by computational methods. We simply note at this point that the structures at all local minima associated with 63-CVE radical anions derived from **3f/3f²⁻** share a common structural feature, with the alkyne vectors tending toward the midpoints of the metal−metal bonds. We return to this point below.

The different voltammograms observed on the CV and bulk electrolysis time scales, but in the absence of any further electrochemical event, strongly suggest the presence of a second dianion, **4²⁻**. Using the calculated geometry of **3f²⁻** as a starting point, one of the alkyne vectors was rotated by 90° and the structure reoptimized, resulting in a second 64-CVE dianion structure, **4f²⁻**, being identified, some 4 kcal/mol more stable than **3f²⁻**. The structure of **4f²⁻** is simply related to that of **3f²⁻** by the reorientation of one of the alkyne vectors (Figure 7). The core geometry of **4f²⁻** is identical to that

Scheme 4

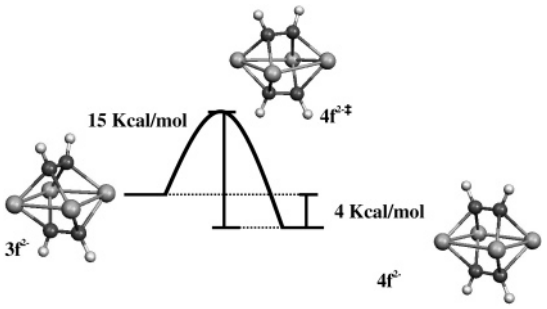

found in the molecular structure of $Ir_4(\mu_4\text{-}MeO_2CC_2CO_2Me)_2(\mu_2\text{-}MeO_2CC_2CO_2Me)_2(CO)_8$, **5**, the only 64-CVE $M_4(alkyne)_2$ cluster to have been crystallographically characterized to date.[12] The optimized geometry of $\mathbf{4f^{2-}}$ has two short Ru−Ru bonds (2.752, 2.736 Å) and two long ones (3.144, 3.014 Å), with the three bridging carbonyls spanning all but the longest Ru−Ru bond (Figure 7, Table 2). Each metal center also carries two terminal carbonyl ligands.

As with $\mathbf{3f^{2-}}$, the excess electron density in $\mathbf{4f^{2-}}$ is relieved by M(d)−C(π*) back-bonding. This back-bonding interaction results in a HOMO that is delocalized over not just the metal centers but also the carbon centers of both alkyne moieties (Figure 7). On the basis of Mulliken population analysis, when compared with **3f**, the additional electron density in $\mathbf{4f^{2-}}$ is distributed over the Ru_4 centers ($0.3e^-$), the carbons centers of the alkyne ligands ($0.5e^-$), and the carbonyl ligands ($1.2e^-$). The reaction pathway between $\mathbf{3f^{2-}}$and $\mathbf{4f^{2-}}$ was examined in some detail to clarify the relationship between these species. A transition state structure calculation was carried out, during which the transient species $\mathbf{4f^{2-‡}}$ was identified, offering an energy barrier to the conversion of ca. 15 kcal/mol (Scheme 4).

In the strictest sense, the static isomers obtained from the optimization process have low symmetry. However, the carbonyl ligands are fluxional on the NMR time scale in the real systems **3** and likely to also be fluxional in the corresponding dianions. If one factors out the location of the carbonyl ligands, the Ru_4C_4 cores of the clusters **3** and the thermodynamically stable form of the dianions $\mathbf{4^{2-}}$ have pseudo C_{2v} and D_{2h} symmetry, respectively. The higher symmetry of the dianions would account for the fewer number of IR active carbonyl bands observed following reduction.

While on the longer time scale of the potentiometric and spectroelectrochemical studies, $\mathbf{4f^{2-}}$ was shown to oxidize back to **3f**, the observation of waves C and D in the faster cyclic voltammetry experiment revealed a more subtle sequence in which $\mathbf{4f^{2-}}$ is oxidized in two one-electron steps, ultimately affording **3f**. The two highest energy filled orbitals in $\mathbf{4f^{2-}}$ are almost isoenergetic and are of A_2 and A_1 symmetry (Figure 7). The A_2 orbital is antisymmetric and is strongly Ru−C bonding, while the A_1 orbital is symmetric and is Ru−Ru bonding. As the two orbitals are within 0.1 eV of each other, oxidation of $\mathbf{4f^{2-}}$ could occur from either of them. If an electron is removed from the A_2 antisymmetric orbital, a decrease in the Ru−C bond strength might be expected. In contrast, the removal of an electron from the A_1 orbital would result only in a small expansion of the metal cluster framework. As noted above, the lower symmetry dianion $\mathbf{3f^{2-}}$ has similar HOMO and HOMO−1 orbitals (Figure 6), and the most distinct difference between the calculated frontier orbitals of $\mathbf{3f^{2-}}$ and $\mathbf{4f^{2-}}$ lies in the varying degree of Ru−C(alkyne) bonding character in the HOMO−1.

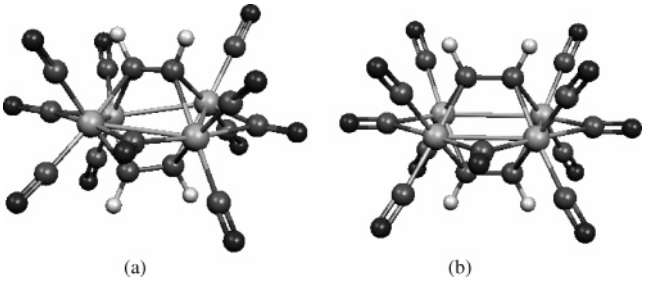

Figure 8. Two of the low-energy structures associated with the 63-CVE radical anion: (a) global minimum derived from removal of an electron from the A_2 orbital of $\mathbf{4f^{2-}}$, (b) a local minimum lying 10 kcal/mol higher in energy derived from removal of an electron from the A_1 orbital of $\mathbf{4f^{2-}}$.

It is rather difficult to resolve definitively the differing behavior of $\mathbf{3f^{2-}}$ and $\mathbf{4f^{2-}}$ upon oxidation (Scheme 2) using computational methods, as the lowest energy conformation on the 63-CVE radical anion potential energy surface will obviously be the same regardless of starting geometry. However, it is interesting to note that regardless of starting geometry employed (**3f**, $\mathbf{3f^{2-}}$, $\mathbf{4f^{2-}}$), all of the local minima encountered during geometry optimization of the 63-CVE radical anion can be summarized in terms of a generic structure in which the alkyne vectors tend toward parallel and are directed toward the midpoints of Ru−Ru bonds. The lowest energy structure identified for the 63-CVE radical anion, generated by removing an electron from the A_2 symmetric orbital of $\mathbf{4f^{2-}}$ and relaxing the geometry, is illustrated in Figure 8, together with a local minimum structure only ca. 10 kcal/mol higher in energy derived from similar removal of the electron from the A_1 symmetric orbital of $\mathbf{4f^{2-}}$. It is obvious that loss of a single electron from $\mathbf{4f^{2-}}$ can be achieved with smaller changes in overall geometry than are necessary with $\mathbf{3f^{2-}}$. The greater structural similarity of $\mathbf{4f^{2-}}$ to the 63-CVE species $\mathbf{4f^-}$ may provide a key to the differing behavior of the dianions on oxidation.

Conclusion

Reduction of the dodecahedral Ru_4C_4 clusters **3** ($E_{1/2}$ ca. −1.5 V), which consumes two electrons, gives $\mathbf{3^{2-}}$. On rapid time scales, the dianion $\mathbf{3^{2-}}$ is cleanly reoxidized to the neutral state, via the pathway shown in Scheme 3, at potentials ca. 1 V more positive than the initial reduction. On longer time scales, $\mathbf{3^{2-}}$ isomerizes to the more thermodynamically stable $\mathbf{4^{2-}}$, which is itself reoxidized in two steps, the first of which also occurs at potentials ca. 1 V more positive than the initial reduction. In both dianions the HOMO is stabilized by back-bonding into the alkyne π*-orbitals, delocalized over not just the metal centers, but also the carbon centers of both alkyne moieties.

(12) Heveldt, P. F.; Johnson, B. F. G.; Lewis, J.; Raithby, P. R.; Sheldrick, G. M. *J. Chem. Soc., Chem. Commun.* **1978**, 340.

Experimental Section

General Conditions. All reactions were carried out under dry high-purity nitrogen using standard Schlenk techniques. Solvents were dried and distilled from conventional agents prior to use. Preparative TLC was performed on 20 × 20 cm glass plates coated with silica gel (Merck GF_{254}, 0.5 mm thick). The complex $[Ru_4(\mu_4\text{-}\eta^2\text{-}PhC_2Ph)(CO)_{12}]$ (**2a**) was prepared by a variation to the literature method,[13] as detailed below. Literature methods were used to prepare $Me_3SiC{\equiv}CC{\equiv}CC{\equiv}CSiMe_3$ (**1b**)[14] and $[Ru_4(\mu_4\text{-}\eta^2\text{-}Me_3SiC{\equiv}CC_2C{\equiv}CSiMe_3)(CO)_{12}]$ (**2b**).[6]

Instrumentation. Infrared spectra were recorded on a Nicolet Avatar FT-IR spectrometer using solution cells of 0.5 mm path length fitted with calcium fluoride windows. NMR spectra were recorded in $CDCl_3$ and referenced against the solvent resonances on Varian Mercury 400 and Varian Inova 500 spectrometers. NMR spectra were recorded in $CDCl_3$ at 399 and 499 MHz (^1H) or 100 and 125 MHz (^{13}C). EI-MS were obtained on an Autospec instrument. FAB-MS were recorded at the EPSRC National Mass Spectrometry Facility, Swansea. Microanalyses were performed at University of Durham using an Exeter Analytical CE−440 elemental analyzer.

Electrochemistry was performed with an EG&G PAR 273 electrochemical analyzer connected to a PC, employing the software M270. A standard three-electrode cell was designed to allow the tip of the reference electrode to closely approach the working electrode. The reference electrode was a saturated calomel electrode (SCE). The working electrode for CV was a glassy carbon (GC) electrode; for polarography a dropping mercury electrode (DME) with flow rate of 1.22 mg s^{-1} at a reservoir height of 0.5 m was employed. Drop time (typically 1 s) was controlled by an electromechanical hammer. The auxiliary electrode was a platinum wire. Positive feedback *iR* compensation was applied routinely. Measurements were carried out under Ar in freshly distilled anhydrous deoxygenated solvents. Solutions were 5×10^{-4} M with respect to the compounds under study and 1×10^{-1} M with respect to the supporting electrolyte, $[Bu_4N][PF_6]$ (Aldrich). The electrolyte was recrystallized three times from 95% ethanol and dried in a vacuum oven at 110 °C overnight prior to use. Potentials (versus SCE) are referred to the ferrocene (0/+1) couple. Under our experimental conditions the Fc/Fc^+ couple was evaluated to be +0.46 V vs SCE in dichloromethane. Each experiment was carried out in duplicate. Spectroelectrochemistry was performed in an optically transparent thin-layer electrochemical (OTTLE) cell assembled as previously described;[15] spectra were recorded on a Bruker Equinox 55 FT-IR spectrometer. The program ESP (C. Nervi) is available free on the Internet at http://lem.ch.unito.it/chemistry/esp_manual.html.

Computational Methods. Geometry optimization, orbital calculations, and transition state calculations were performed using the B3LYP functional[16] as implemented within the Gaussian 98 software package,[17] with a 3-21G* basis set for ruthenium and a 6-31G** basis set for all other atoms. At the time we began this study, the structure of **3f** had not been reported, and the coordinates from the structure of **3a** were used as a starting geometry. Default criteria within the software were employed for geometry optimization, which places an uncertainty of less than ±0.005 Å on bond lengths. The dependence of the calculation upon basis set was tested using the TZVP basis set, and also with the Los Alamos effective core potentials and associated basis set (LACVP**). Results of these calculations were in qualitative agreement with those reported here, although we note that in the latter calculation $\mathbf{3f}^{2-}$ and $\mathbf{4f}^{2-}$ are isoenergetic. Thus, overall we have confidence that the qualitative picture of the chemistry is converged with respect to this parameter. Initial structural optimizations were performed in point group C_1, after which the coordinates were symmetrized, and the structure was reoptimized in the appropriate point group (even though the symmetrized structures had very low gradients). Frequency analysis was carried out for all reported structures where isomers were found to have $(3n-6)$ positive vibrational eigenvalues and the transition states were found to have one imaginary vibrational eigenvalue. Finally, the results of the orbital calculations were displayed graphically using the Molekel software package.[18]

$Ru_4(\mu_4\text{-}\eta^2\text{-}PhC_2Ph)(CO)_{12}$ (2a). Powdered $Ru_3(CO)_{12}$ (0.2 g, 0.27 mmol) was suspended in hexane (20 mL) and treated with diphenylacetylene (0.05 g, 0.28 mmol). The orange solution was heated at reflux for 6 h, cooled, and filtered to remove residual $Ru_3(CO)_{12}$. The filtrate was evaporated and the residue purified by column chromatography (silica gel, hexane/CH_2Cl_2 gradient). The product was eluted with 5% CH_2Cl_2/hexane as a brown band (second band) and crystallized from hexane (0.07 g, 0.06 mmol, 24%).

$Ru_4(\mu_4\text{-}\eta^2\text{-}PhC_2Ph)_2(CO)_{11}$ (3a). A solution of $Ru_4(CO)_{12}(\mu_4\text{-}\eta^2\text{-}PhC_2Ph)$ (**2a**) (0.07 g, 0.06 mmol) in hexane (20 mL) was treated with diphenylacetylene (0.02 g, 0.11 mmol) and heated at reflux for 6 h. The solution was cooled and a red precipitate collected by filtration. The filtrate was heated at reflux overnight with additional diphenylacetylene (0.02 g, 0.11 mmol) to give a second crop of product. The combined precipitate (0.05 g, 0.05 mmol, 51%) was recrystallized from CH_2Cl_2/MeOH (51%). IR (cyclohexane): ν(CO) 2085 m, 2055 ms, 2040 s, 2023 s, 1981 ms, 1835 m cm^{-1} [lit.[10] (CH_2Cl_2) 2084 w, 2070 vw(sh), 2054 w, 2041 vs, 2025 s, 1982 m, 1942 m, 1836 w,br cm^{-1}]. ^1H NMR: δ 6.71 (d, 8H, Ph), 6.93 (q, 12H, Ph). ^{13}C NMR: δ 126.67 (C_2), 127.23, 128.56, 144.81, 148.08 (4 × Ph), 199.09 (CO). FAB-MS (*m/z*): 1014 $[M - 2CO]^+$, 986−762 $[M - nCO]^+$ $n = 3-9$.

$Ru_4(\mu_4\text{-}\eta^2\text{-}Me_3SiC{\equiv}CC_2C{\equiv}CSiMe_3)(\mu_4\text{-}\eta^2\text{-}PhC_2Ph)(CO)_{11}$ (3b). A solution of $Ru_4(\mu_4\text{-}\eta^2\text{-}Me_3SiC{\equiv}CC_2C{\equiv}CSiMe_3)(CO)_{12}$ (**2b**) (0.56 g, 0.55 mmol) in hexane (20 mL) was treated with diphenylacetylene (0.58 g, 2.07 mmol), the solution was refluxed for 8 h and cooled, and the solvent was removed. The crude product was purified by preparative TLC (hexane). The orange band contained the desired product and was recrystallized from CH_2Cl_2/hexane (0.32 g, 0.27 mmol, 49%). IR (cyclohexane): ν(C≡C) 2130 w, ν(CO) 2088 w, 2074 w, 2063 s, 2050 s, 2043 m, 2029 m, 1998 m, 1981 m cm^{-1}. FAB-MS (*m/z*): 1052 $[M - 2CO]^+$, 1024−800 $[M - nCO]^+$ $n = 3-11$. Anal. Calcd for $Ru_4Si_2O_{11}C_{37}H_{28}$: C 40.07, H 2.54. Found: C 39.60, H 2.77.

$Ru_4(\mu_4\text{-}\eta^2\text{-}Me_3SiC{\equiv}CC_2C{\equiv}CSiMe_3)_2(CO)_{11}$ (3c). A solution of $Ru_4(\mu_4\text{-}\eta^2\text{-}Me_3SiC{\equiv}CC_2C{\equiv}CSiMe_3)(CO)_{12}$ (**2b**) (0.14 g, 0.13 mmol) in hexane (20 mL) was treated with $Me_3SiC{\equiv}CC{\equiv}CC{\equiv}CSiMe_3$ (0.13 g, 0.46 mmol), the solution was heated at reflux point for 8 h and cooled, and the solvent was removed. The crude product was purified by preparative TLC (hexane). The orange band contained the desired product and was

(13) Wang, J.; Sabat, M.; Lyons, L. J.; Shriver, D. F. *Inorg. Chem.* **1991**, *30*, 382.
(14) Rubin, Y.; Lin, S. S.; Knobler, C. B.; Anthony, J.; Boldi, A. M.; Diederich, F. *J. Am. Chem. Soc.* **1991**, *113*, 6943.
(15) Krejcik, M.; Danek, M.; Hartl, F. *J. Electroanal. Chem.* **1991**, *317*, 179.
(16) Becke, A. D. *J. Chem. Phys.* **1993**, *98*, 5648.
(17) Frisch, M. J.; Trucks, G. W.; Schlegel, H. B.; Scuseria, G. E.; Robb, M. A.; Cheeseman, J. R.; Zakrzewski, V. G.; Montgomery, Jr., J. A.; Stratmann, R. E.; Burant, J. C.; Dapprich, S.; Millam, J. M.; Daniels, A. D.; Kudin, K. N.; Strain, M. C.; Farkas, O.; Tomasi, J.; Barone, V.; Cossi, M.; Cammi, R.; Mennucci, B.; Pomelli, C.; Adamo, C.; Clifford, S.; Ochterski, J.; Petersson, G. A.; Ayalao, P. Y.; Cui, Q.; Morokuma, K.; Malick, D. K.; Rabuck, A. D.; Raghavachari, K.; Foresman, J. B.; Cioslowski, J.; Oritz, J. V.; Stefanov, B. B.; Liu, G.; Liashenko, A.; Piskorz, P.; Komaromi, I.; Gomperts, R.; Martin, R. L.; Fox, D. J.; Keith, T.; Al-Laham, M. A.; Peng, C. Y.; Nanayakkara, A.; Gonzalez, C.; Challacombe, M.; Gill, P. M. W.; Johnson, B.; Chen, W.; Wong, M. W.; Andres, J. L.; Gonzalez, C.; Head-Gordon, M.; Replogle, E. S.; Pople, J. A. *Gaussian 98*, Revision A.3; Gaussian, Inc.: Pittsburgh, PA, 1998.
(18) Flükiger, Lüthi, H. P.; Weber, J. *Molekel*, Revision 4.0; Swiss Center for Scientific Computing: Manno Switzerland, 2000.

recrystallized from CH_2Cl_2/hexane (0.04 g, 0.03 mmol, 23%). IR (cyclohexane): ν(C≡C) 2158 w, 2131 m, ν(CO) 2088 s, 2064 s, 2040 s, 2027 s, 2008 s, 1854 m cm^{-1}. ^1H NMR: δ 0.03 (s, 36H, $SiMe_3$). ^{13}C NMR: δ 0.03 ($SiMe_3$), 113.00 (C_2), 97.83, 109.61, (2 × C≡C), 197.91 (CO). FAB-MS (*m/z*): 1149 $[M]^+$, 1121−897 $[M - nCO]^+$ n = 2−9. Anal. Calcd for $Ru_4Si_4O_{11}C_{35}H_{36}$: C 36.58, H 3.16. Found: C 36.21, H 3.27.

$Ru_4(\mu_4\text{-}\eta^2\text{-}Me_3SiC{\equiv}CC_2C{\equiv}CSiMe_3)(Me_3SiC_2C{\equiv}CSiMe_3)(CO)_{11}$ (3d). A solution of $Ru_4(\mu_4\text{-}\eta^2\text{-}Me_3SiC{\equiv}CC_2C{\equiv}CSiMe_3)(CO)_{12}$ (**2b**) (0.05 g, 0.056 mmol) in hexane (10 mL) was treated with $Me_3SiC{\equiv}CC{\equiv}CSiMe_3$ (0.03 g, 0.162 mmol), the solution was heated at reflux for 6 h and cooled, and the solvent was removed. The crude product was purified by preparative TLC (5% CH_2Cl_2/hexane). The major yellow band contained the desired product and was recrystallized from $CHCl_3$/hexane (0.03 g, 0.02 mmol, 45%) to afford orange block-shaped crystals. IR (cyclohexane): ν(C≡C) 2130 w, ν(CO) 2092 s, 2067 s, 2060 s, 2027 s, 1989 s, 1975 s, 1850 s cm^{-1}. ^1H NMR: δ 0.04 (s, 18H, $SiMe_3$), 0.07 (s, 9H, $SiMe_3$), 0.18 (s, 9H, $SiMe_3$). ^{13}C NMR: δ −1.05, −0.39, 5.91 (3 × $SiMe_3$), 112.26, 114.68, 141.14 (3 × C_2), 96.57, 104.50, 109.71, 110.43, (4 × C≡C), 198.85 (CO). FAB-MS (*m/z*): 1125 $[M]^+$, 1097−817 $[M - nCO]^+$ n = 1−11. Anal. Calcd for $Ru_4Si_4O_{11}C_{33}H_{36}$: C 35.23, H 3.20. Found: C 34.86, H 3.26.

Crystallography. 3b. Data were collected on a Bruker SMART-CCD 6000 diffractometer (ω-scan, 0.3°/frame) yielding 18 870 unique data (R_{merg} = 0.066). The structure was solved by direct methods and refined by full-matrix least squares on F^2 for all data using SHELXTL software. All non-hydrogen atoms were refined with anisotropic displacement parameters; H atoms were placed into the calculated positions and refined using a "riding" model. Final $wR_2(F^2)$ = 0.1123 for all data (399 refined parameters), conventional $R_1(F)$ = 0.0469 for 13 462 reflections with $I \geq 2\sigma$, GOF = 1.037. The largest peak on the residual map (2.15 e/Å^3) is located close to one of the Ru atoms and, obviously, is the result of truncation of the Fourier series. Crystallographic data for the structure have been deposited with the Cambridge Crystallographic Data Centre (CCDC-262964).

3d. Data were collected on a Siemens Smart CCD diffractometer at −100 °C, using graphite-monochromatized Mo Kα radiation (λ = 0.71073 Å) in the ω scan mode. The unit cell was determined from randomly selected reflections obtained using the SMART CCD automatic search, center, index, and least squares routines. Integration was carried out using the program SAINT, and an absorption correction was performed using SADABS.[19] The crystal structures were solved by direct methods, and the structure was refined by full-matrix least squares routines using the SHELXTL program suite.[20] All atoms were refined anisotropically. All distances and angles in disordered parts (the C(40)−C(41)−Si(1) chain is disordered over three sites with occupancy 0.23, 0.27, 0.5, and CO(10) and CO(11) ligands are disordered over two positions with equal occupancy) were fixed. Hydrogen atoms were placed in calculated positions and allowed to ride on the parent atoms. Crystallographic data for the structure have been deposited with the Cambridge Crystallographic Data Centre (CCDC-263009).

Acknowledgment. This work was supported by the EPSRC and the University of Durham (P.J.L., J.A.K.H.). C.N. gratefully acknowledges financial support from MURST (Rome, COFIN99). O.F.K. held an Isobelle Fleck Scholarship (University of Durham) and an Overseas Research Award. FAB mass spectra were provided by the EPSRC National Mass Spectrometry Service (Swansea). A generous loan of $RuCl_3{\cdot}nH_2O$ from Johnson Mathey Plc, Reading, is gratefully acknowledged. We would also like to thank the reviewers for several helpful comments and suggestions.

Supporting Information Available: A complete listing of the crystal data and refinement parameters, atomic coordinates, and equivalent isotropic displacement parameters, bond lengths and angles, anisotropic displacement parameters, and hydrogen coordinates and isotropic displacement parameters for complexes **3b** and **3d**. A description of the electrochemical simulations and results is also available. This material is available free of charge via the Internet at http://pubs.acs.org.

OM049457Y

(19) Sheldrick, G. M. *SADABS* Version 2.03; University of Gottingen: Germany, 2002.

(20) Sheldrick, G. M. *SHELXTL*, Version 6.10; Bruker AXS Inc.: Madison, WI, 2000.